Spitzer IRS Spectra of Optically Faint IRAS Sources

Lusine Sargsyan[1], Areg Mickaelian[1], Daniel Weedman[2], James Houck[2]

ABSTRACT

Extragalactic sources from the IRAS Faint Source Catalog (FSC) which have the optically faintest magnitudes ($E \gtrsim 18$) were selected by spatial coincidence with a source in the FIRST radio survey, and 28 of these sources have been observed with the Infrared Spectrograph on *Spitzer* (IRS). While an infrared source is always detected with the IRS at the FIRST position, only $\sim 50\%$ of the infrared sources are real FSC detections, as estimated from the number of sources for which the $f_\nu(25\ \mu\mathrm{m})$ determined with the IRS is fainter than the sensitivity limit for the FSC. Sources have $0.12 < z < 1.0$ and luminosities (ergs s^{-1}) $43.3 < \log[\nu L_\nu(5.5\ \mu\mathrm{m})] < 46.7$, encompassing the range from local ULIRGs to the most luminous sources discovered by *Spitzer* at z $\sim$ 2. Detectable PAH features are found in 15 of the sources (54%), and measurable silicate absorption is found in 19 sources (68%); both PAH emission and silicate absorption are present in 11 sources. PAH luminosities are used to determine the starburst fraction of bolometric luminosity, and model predictions for a dusty torus are used to determine the AGN fraction of luminosity in all sources based on $\nu L_\nu(5.5\ \mu\mathrm{m})$. Approximately half of the sources have luminosity dominated by an AGN and approximately half by a starburst. The ratio of infrared to radio flux, defined as q = $\log[f_\nu(25\ \mu\mathrm{m})/f_\nu(1.4\ \mathrm{GHz})]$, does not distinguish between AGN and starburst for these sources.

Subject headings: infrared: galaxies — galaxies: starburst— galaxies: AGN

1. Introduction

As part of efforts to determine the nature of faint infrared sources, hundreds of spectra have been obtained with the Infrared Spectrograph on *Spitzer* (IRS; Houck et al. 2004)

[1]Byurakan Astrophysical Observatory (BAO) and Isaac Newton Institute (INI) of Chile, Armenian Branch, Byurakan 378433, Aragatzotn province, Armenia; sarl11@yahoo.com

[2]Astronomy Department, Cornell University, Ithaca, NY 14853; dweedman@astro.cornell.edu

of optically faint sources discovered at 24 μm with surveys using the Multiband Imaging Photometer (MIPS; Rieke et al. 2004). The most important result is that these faint sources having $f_\nu(24\ \mu\mathrm{m}) \sim 1$ mJy are generally at high redshift, typically z $\sim$ 2 (Houck et al. 2005; Weedman et al. 2006a,b; Yan et al. 2007; Brand et al. 2007). Most show the 9.7 μm silicate absorption feature, but some have PAH emission features and some have only a continuum with no detectable features. These results imply that the sources are optically faint because they are both distant and obscured by dust.

The absorbed sources and the featureless, power-law sources have been interpreted as obscured AGN (Sajina et al. 2007; Polletta et al. 2007). This interpretation implies that the surface density of optically obscured AGN at high redshifts exceeds that for classical, optically discoverable AGN by a factor of two to three in infrared surveys to $f_\nu(24\ \mu\mathrm{m}) \lesssim$ 1 mJy (Weedman et al. 2006c; Polletta et al. 2007; Fiore et al. 2007). Extremely luminous starbursts have also been found at z $\sim$ 2 (Farrah et al. 2008; Pope et al. 2008) which appear similar to local starbursts in all characteristics except luminosity.

To understand these high redshift, dusty sources and to interpret the *Spitzer*-discovered sources within scenarios for evolution in the universe, it is essential to understand how the sources of luminosity are distributed between AGN and starbursts among the overall population of sources. This requires comparison with closer, brighter examples for which AGN and starburst diagnostics within the IRS spectra can be compared to information from other wavelengths. So far, the comparison samples which show the most similar spectral shapes are the ULIRGS (Hao et al. 2007; Imanishi et al. 2007; Farrah et al. 2007; Desai et al. 2007), but the ULIRGs have lower luminosities and smaller redshifts than the sources at z $\sim$ 2. The ULIRGS observed with the IRS were chosen primarily on the basis of 60 μm fluxes from the Infrared Astronomical Satellite (IRAS) and were not selected based on optical characteristics.

In this paper, we describe a sample of optically faint, infrared-bright galaxies which spans luminosities and redshifts between the ULIRG and high redshift *Spitzer* IRS samples. This new sample arises from selecting the optically faintest sources listed in the IRAS Faint Source Catalog (FSC)(Moshir et al. 1990). These sources have $E \gtrsim 18$ mag (the photographic E magnitude band is centered at 0.66 μm and approximately corresponds to R magnitude (Humphreys et al. 1991)).

As an additional selection criterion, we also require that the source be present in the FIRST radio survey (Becker et al. 1997; White et al. 1997). The requirement of a radio detection was used to increase confidence that an FSC source is real (as opposed to noise or cirrus) and to provide an accurate position for selection of the optical counterpart.

New IRS spectra of 24 sources and 4 spectra of archival sources are presented. This sample of 28 sources is compared to previous samples of bright IRAS sources for which *Spitzer* IRS spectroscopy is available, and the validity of the FSC identifications is discussed. Spectral parameters are used to estimate starburst and AGN contributions to the luminosity.

2. Sample Selection and Data Analysis

2.1. Selection of New Sample of Infrared Bright, Optically Faint Sources

To select a sample of optically faint infrared sources from the IRAS FSC, we first cross-correlated the IRAS FSC sources with the FIRST catalog, using FSC sources listed as real detections rather than upper limits at both 25 μm and 60 μm (sources with quality flags 2 or 3). 2,310 sources were associated to within 3 times the FSC one sigma positional uncertainty (ranging from 15″to 90″for individual sources). Images from the Palomar Second Digitized Sky Survey (DSS2) were then examined for the 2,310 fields to determine an optical identification at the radio source position.

Of the 2,310 sources, 1,944 can be identified with bright or medium brightness galaxies (photographic $E \lesssim 16$ mag), and 225 are fainter galaxies (16 mag $\gtrsim E \lesssim 21$ mag). The remaining 141 sources are identified with bright Galactic stars or have no optically identifiable galaxy; the latter could be either spurious sources or cirrus sources.

The best available optical photometry for the entire FSC sample is the Minnesota APS catalog (Cabanela et al. 2003), which gives photographic O and E magnitudes. The final sample we select is defined by having $E > 18$. While actual magnitudes are uncertain to a few-tenths, we can have confidence that the APS magnitudes are homogeneous and allow location of the optically faintest sources. The selection for $E > 18$ yields 31 sources, which is about 1% of all sources common between FSC and FIRST.

2.2. IRS Observations and Analysis

We have obtained IRS low-resolution spectra for 24 of these 31 sources, and an additional 4 have been observed in other *Spitzer* programs. The sample of objects and the details of the *Spitzer* IRS[1] observations are in Table 1. Our new observations were made with the

[1] The IRS was a collaborative venture between Cornell University and Ball Aerospace Corporation funded by NASA through the Jet Propulsion Laboratory and the Ames Research Center.

IRS Short Low module in orders 1 and 2 (SL1 and SL2) and with the Long Low module in orders 1 and 2 (LL1 and LL2), described in Houck et al. (2004). These give low resolution spectral coverage from ∼5 μm to ∼35 μm .

Sources were placed on the slit by using the IRS peakup mode with the red camera. Background subtraction for spectra was done using coadded background images that added both nod positions having the source in the other slit (i.e., both nods on the LL1 slit when the source is in the LL2 slit produce LL1 spectra of background only). This subtraction is possible when both SL orders or both LL orders are observed with the same integration times. Independent extractions of spectra at the two nod positions were compared to reject any highly outlying pixels in either spectrum, and a final mean spectrum was produced.

Starting with v15 of the SSC basic calibrated data (BCD), spectra were extracted using the SMART analysis package (Higdon et al. 2004). Extractions were done with an average width of 4 pixels (perpendicular to dispersion; width varies with wavelength because of varying spatial resolution). Calibrations applied to BCD products use extractions of 8 pixel width for the calibrating stars, so we correct fluxes by using Markarian 231 as a standard source and extracting it with both 8 pixel and 4 pixel windows. Final spectra were boxcar-smoothed to the approximate resolution of the different IRS modules (0.2 μm for SL1 and SL2, 0.3 μm for LL2, and 0.4 μm for LL1). All spectra are illustrated in Figures 1-4, ordered by luminosity.

Measured continuum parameters and feature strengths for the spectra are in Table 2. Fluxes and equivalent widths (EWs) for the 6.2 μm and 11.3 μm PAH features are measured using the single Gaussian line fit routine within SMART. For the 6.2 μm PAH line, the fitting is between 5.5 μm and 6.9 μm ; for the 11.3 μm line, fitting is between 10.4 μm and 12.2 μm .

As discussed by Brandl et al. (2006) and Pope et al. (2008), fluxes and EWs of PAH features depend on the underlying continuum level which is selected. This is not a straight-forward choice and is more uncertain for the blended 7.7 μm feature than for the individual 6.2 μm and 11.3 μm features. To minimize uncertainties based on assumptions for fitting the features, we do not list measurements for the 7.7 μm line.

The fitting procedure we use applies a linear fit for the continuum and a Gaussian fit for the line between the selected wavelengths. This linear continuum fit is somewhat different from the spline fit used by Brandl et al. (2006) and yields a higher continuum level. To estimate uncertainties arising from the fitting procedure, we remeasured the Brandl starbursts with the procedure we use. Using the 17 starbursts having single components (so there is no uncertainty regarding what flux to include in the spectral extraction), the average EW of the 6.2 μm feature given by Brandl et al. (2006) is greater by 1.11 then the EWs we measure.

In Table 2, the parameter τ_{si} describing the depth of the 9.7 μm silicate absorption feature is measured using the continuum fitting technique described by Spoon et al. (2007). The average spectrum of the 19 sources showing silicate absorption is compared to the spectrum of Markarian 231 in Figure 5.

We note that Source 9 is a blazar (Perry et al. 1978) with observed IRS flux at 25 μm smaller by a factor of 30 than when observed by IRAS. The source met the criteria for definition of the sample and so was observed, but this source is not included in the luminosity plots. As a result of the unexpectedly low flux, the IRS spectrum is very noisy and shows no measurable features (Figure 4). PAH limits are not meaningful for this source compared to those for other sources.

3. Discussion

3.1. Reality of IRAS FSC Sources

The optically faint sources chosen are often near the lower limit of f_ν(25 μm) in the IRAS FSC; the mean FSC f_ν(25 μm) of the sources chosen is 150 mJy, but the typical one sigma noise for an FSC source is 65 mJy. At this low signal to noise, some of these sources may be spurious. They could appear in the FSC catalog either because of enhancing noise or because of confusing Galactic cirrus.

To test the reality of the FSC sources, we determined what should be the IRAS f_ν(25 μm) by applying a synthesized IRAS filter to the *Spitzer* IRS spectrum, using the synthesis tool in SMART. The resulting IRS f_ν(25 μm) are listed in Table 2. In Figure 6, the IRAS f_ν(25 μm) and the synthetic IRS f_ν(25 μm) are compared.

Fig. 6 shows that the f_ν(25 μm) from IRAS are always greater than the f_ν(25 μm) measured with the *Spitzer* IRS, with a median factor of 1.6 and extending to a factor of 6. The discrepancy increases with decreasing flux, so that the faintest sources show the largest ratio of IRAS to *Spitzer* flux. Various previous observations with comparable IRS signal to noise indicate internal consistency of *Spitzer* MIPS and IRS fluxes at 24 μm to within 5% (Houck et al. 2007), so IRS flux calibration uncertainty is much less than the differences observed with IRAS fluxes.

One possible source of difference arises when the IRAS source is larger than the IRS slit so that so that some flux is omitted in the IRS spectrum. This is the case for many nearby starbursts in Brandl et al. (2006). Images of the FSC sources were obtained at $\sim$

25 μm because acquisition of sources used the IRS red peakup camera, and all images show an unresolved source as evidenced by the presence of a diffraction ring. This indicates that extended sources cannot explain the differences between IRAS and IRS fluxes.

We conclude that the differences between IRAS and IRS fluxes arise because many of these sources are near the detection limit for the IRAS FSC. Fig. 6 shows that 14 of the IRAS FSC sources are actually fainter at 25 μm, as measured by IRS f_ν(25 μm), than the typical one sigma sensitivity limit of 65 mJy quoted for the FSC. This implies that these faint FSC "detections" are spurious, perhaps accidental noise spikes.

Therefore, we use the ratio IRAS f_ν(25 μm)/IRS f_ν(25 μm) to estimate the reality of the IRAS FSC source. If this ratio is < 1.5, we assume the source is really detected in the IRAS FSC, because flux discrepancies of this amount are reasonable for the faint FSC sources. Also, this is the approximate flux ratio at which the IRAS FSC fluxes fall below the 65 mJy sensitivity limit in Figure 6. By this criterion, 14 (50%) of the sources are real FSC detections (counting the blazar for which the flux discrepancy is attributed to variability).

If half of the FSC infrared sources are not real, why did all of the FSC sources appear as *Spitzer* sources? We believe that the answer is because the requirement of a FIRST radio source at the IRAS FSC position was also a criterion for source selection. As shown below, *Spitzer* sensitivities are such that a *Spitzer* source should be detected for any radio source brighter than the FIRST limit, regardless of whether the source was actually detected in the IRAS FSC.

The ratio of infrared to radio flux is described by the parameter q = log[f_ν(25 μm)/f_ν(1.4 GHz)]. The median q = 0.8 for faint *Spitzer* sources detected at both 24 μm and 1.4 GHz (Appleton et al. 2004), and this is also the q value expected from previously known radio-infrared correlations for starbursts (Condon et al. 1982). The FIRST catalogue includes sources to a point-source limit of 1 mJy for typical one sigma rms of 0.13 mJy (White et al. 1997). This limit means that a *Spitzer* source would have been found with f_ν(25 μm) > 6 mJy for any FIRST source with q > 0.8. Such a source would be detectable by the peakup pointing of *Spitzer*, and an IRS spectrum would be obtained, even if the FSC detection were not real.

This result means that any FIRST source with an infrared to radio ratio exceeding the median expected value would be detected in our *Spitzer* pointings. The existence of a FIRST source makes it probable, therefore, that a detectable *Spitzer* source would be found even if the FSC source used for the initial identification were not real. This explains why *Spitzer* sources were always found at the FIRST position even in those cases when the f_ν(25 μm) are too faint for the FSC detection to be real.

3.2. Characteristics of Spectra and Near-Infrared Luminosities

Spectra of the FSC sample are shown in Figures 1 through 4, ordered by $\nu L_\nu(5.5\ \mu m)$, with lowest luminosity sources shown first. This ordering allows some overall spectral trends to be seen. Sources with the strongest PAH features and weakest silicate absorption (sources 15, 5, and 7) are among the lowest luminosity sources, in Figure 1. Sources of intermediate luminosity, in Figures 2 and 3, generally show conspicuous silicate absorption and weak PAH features. Finally, the highest luminosity sources (Figure 4) have the weakest silicate absorption and the weakest PAH features.

As a comparison standard throughout, we use the thoroughly studied ULIRG Markarian 231 because its mid infrared spectrum (Weedman et al. 2005; Armus et al. 2007) is similar in shape to many other absorbed sources. In Figure 5, we show this similarity by comparing the average spectrum of all the FSC sources in Table 2 having silicate absorption to the spectrum of Markarian 231. The average absorption depth is similar to that of Markarian 231, for which the silicate optical depth of -0.7 corresponds to maximum extinction by the silicate feature of $\sim$ 50% of the continuum flux.

The distribution of continuum luminosities for the FSC sources is shown in Figure 7, based on $\nu L_\nu(5.5\ \mu m)$. This parameter is chosen for comparison to the large samples of ULIRGs, Sy1, Sy2, and QSOs summarized in Hao et al. (2007). All of these sources previously observed with the IRS have $\log[\nu L_\nu(5.5\ \mu m)] < 46.1$, and the median ULIRG luminosity is $\log[\nu L_\nu(5.5\ \mu m)] = 44.4$. The luminosity limit of these previously observed sources is exceeded by 3 of the FSC sources. The most luminous obscured sources at z $\sim$ 2 (Houck et al. 2005; Yan et al. 2007) have $\log[\nu L_\nu(5.5\ \mu m)] < 46.6$ (Polletta et al. 2007), and this extreme luminosity is matched by one of the FSC sources. The median luminosity of the FSC sources in Figure 7 is $\log[\nu L_\nu(5.5\ \mu m)] = 44.8$. These results indicate, therefore, that the FSC sample encompasses a luminosity range which includes typical ULIRGs and extends to the most luminous sources discovered by *Spitzer*.

3.3. Comparison of FSC Sample to Previous ULIRG samples

One objective of the present study was to assemble a sample of IRAS sources substantially fainter in infrared and optical flux than the luminous ULIRGS defined by the IRAS 1 Jy survey (Kim et al. 1998) whose IRS spectra are discussed by Imanishi et al. (2007), Farrah et al. (2007), and Desai et al. (2007). Objectives include learning how the nature of IRAS sources changes as flux becomes fainter, and especially to seek sources that are more similar in luminosity and redshift to the high-redshift sources discovered in *Spitzer* surveys of sources at ~ 1 mJy.

The FSC sample was chosen to have the faintest optical magnitudes that could be found in the FSC in order to select the IRAS sources with the most extreme values of observed infrared to optical flux ratio (IR/opt). The faint *Spitzer* samples in Bootes (Houck et al. 2005) and the FLS (Yan et al. 2007) have typical $R \sim 25$ mag and $f_\nu(25\ \mu\mathrm{m}) \sim 1$ mJy. In the observer's frame, objects having similar IR/opt in the FSC, with typical $f_\nu(25\ \mu\mathrm{m})$ ~ 100 mJy, should have $R > 20$ mag. Very few FSC objects are so faint and so extreme in IR/opt, but all sources in Table 1 have photographic $E > 18$. (We assume within the magnitude uncertainties that E and R are similar).

Figure 8 compares the FSC sample and the ULIRG samples in $25\,\mu$m flux and redshift (using the *Spitzer* IRS $f_\nu(25\ \mu\mathrm{m})$ for the FSC sources and the IRAS $f_\nu(25\ \mu\mathrm{m})$ for the ULIRG sources). The FSC sample extends to higher redshifts than the previously published ULIRG samples which have IRS spectra. The maximum redshift of the FSC sample is 0.93 with median redshift of 0.25 whereas the ULIRG samples tabulated by Imanishi et al. (2007) and Farrah et al. (2007) have maximum z of 0.26. The combined dataset extends over a range of nearly 1000 in $f_\nu(25\ \mu\mathrm{m})$.

The ratio of mid-infrared to optical or near-infrared flux is a measure of how much a source is dominated by dust absorption and dust continuum luminosity. In general, very dusty sources will have ratios enhanced both by increased extinction of shorter wavelengths and increased dust continuum at longer wavelengths, although detailed understanding of individual sources requires modeling of the dust absorption and emission contributions (e.g. Marshall et al. 2007). For comparing fluxes at different wavelengths among samples, homogeneous all-sky data measuring optical magnitudes for IRAS sources are not available other than the photographic magnitudes used for our initial selection. However, the 2MASS survey (Skrutskie et al. 2006) encompasses all sources in the ULIRG samples and most sources in our FSC sample with near-infrared J,H,K photometry.

In Figure 9, the flux distributions at $25\,\mu$m and ratio $f_\nu(25\ \mu\mathrm{m})/f_\nu(\mathrm{J})$ for the FSC sample are compared with the ULIRG samples in Imanishi et al. (2007) and Farrah et al. (2007). (The flux transformation adopted for 2MASS J mag is that zero magnitude corresponds to 1590 Jy.) The median for the combined ULIRG samples is $f_\nu(25\ \mu\mathrm{m})/f_\nu(\mathrm{J}) = 2.42$ and is the same for the FSC sample, counting limits. Although the FSC sample was chosen for faint optical magnitudes, this similarity in $f_\nu(25\ \mu\mathrm{m})/f_\nu(\mathrm{J})$ indicates that the FSC sample does not select in favor of sources with a greater dust content compared to the ULIRG samples. The FSC sample does contain sources at greater redshifts than the Imanishi et al. (2007) and Farrah et al. (2007) ULIRG samples, as shown in Fig. 8, although this result arises in part because the Imanishi et al. (2007) sample was restricted to ULIRGs with z < 0.15.

3.4. Luminosities from AGN and Starbursts

One major objective of previous ULIRG studies has been to determine the relative contributions of starbursts and AGN to the total luminosity of a source. A division of luminosity between starbursts and AGN at rest frame $\sim 6\,\mu$m can be determined by the strength of the PAH features compared to the continuum, as measured by the equivalent width (EW) of the PAH features (Genzel et al. 1998; Laurent et al. 2000; Imanishi et al. 2007; Farrah et al. 2007; Desai et al. 2007). Pure starbursts with no indicators of AGN at any wavelength have rest frame EW(6.2 μm) > 0.45 (Brandl et al. 2006). Smaller equivalent widths correspond to an increasing continuum, assumed to be caused by an AGN. Very few ULIRGS have such strong PAH features; only 2 of 49 in Imanishi et al. (2007) and 8 of 107 in Desai et al. (2007), which indicates a substantial AGN contribution to the continuum at $6\,\mu$m .

The distribution of PAH strength for the FSC sample is shown in Figure 7; only one of 28 sources has $6.2\,\mu$m EW > 0.45 and only three have EW > 0.2. These results indicate that, as in the ULIRG samples, the near-infrared continuum is generally much stronger relative to the PAH feature than in pure starbursts. It is also seen in Figure 7 that the most luminous sources at rest frame $5.5\,\mu$m in the FSC sample are sources with the smallest PAH equivalent widths. The simplest interpretation of these results is that the most luminous near-infrared sources are dominated by AGN power.

How the luminosity divides in the near-infrared between AGN and starbursts is not necessarily the same as the separation of starburst and AGN power for bolometric luminosities. Many efforts have been made to separate the bolometric contributions within ULIRGs of AGN and starbursts by assuming templates for the total AGN spectrum and the total starburst spectrum (e.g. Farrah et al. 2003). In general, results are that the far infrared luminosity from cooler dust is attributed primarily to the starburst whereas the near infrared luminosity from warmer dust is attributed to an AGN. The warmer AGN contribution leads to stronger near infrared continuum than from starbursts, causing the low equivalent widths for PAH features.

Assumed templates can be incorrect if, for example, there is cooler dust outside of the dusty torus which is also heated by the AGN, or if starbursts are deeply buried in optically thick clouds that produce hotter dust (e.g. Levenson et al. 2007; Imanishi et al. 2007; Polletta et al. 2007). The templates may be examples of observed sources, but the intrinsic nature of the template sources may not be fully understood. It is desirable, therefore, to determine an estimate of AGN and starburst contributions which is independent of template assumptions.

For the rest frame parameters $\nu L_\nu(5.5\ \mu m)$ and L(6.2 μm), which are measured for our sources in Table 3, empirical determinations relate these parameters to the bolometric luminosities of obscured AGN [L_{ir}(AGN)] and of starbursts [L_{ir}(SB)]. For local starbursts (Brandl et al. 2006) and high redshift submillimeter galaxies which are starbursts (Pope et al. 2008), an empirical relation has been found to be $\log[L_{ir}(SB)] = \log[L(6.2\ \mu m)] + 2.7 \pm 0.1$; L(6.2 μm) is the total luminosity of the 6.2 μm PAH feature, after subtracting the underlying continuum.

This result derives from an observational comparison of PAH luminosity and bolometric luminosity; while there may be some extinction of the 6.2 μm feature, effects of extinction would be included in the empirical result. Adopting this relation also assumes that L(6.2 μm) is measured the same in all sources. The uncertainty listed does not include the $\sim 10\%$ systematic uncertainty in measurement of 6.2 μm fluxes that may arise from differences in the fitting procedure discused in section 2.2. Pope et al. (2008) state that their measures are "consistent" with those of Brandl et al. (2006), to which we also compare in section 2.2. Because our measures agree within 10% of the Brandl measures, we adopt the relation in Pope et al. (2008) without applying a systematic correction. This relation applies to a "pure" starburst, with no AGN contribution to infrared luminosity.

For AGN, it is assumed that the infrared continuum associated with the AGN arises from warm dust within a torus surrounding the accretion region. Using the clumpy torus model of Hönig et al. (2006), empirical fits to overall SEDs in Polletta et al. (2007) give $\log[L_{ir}(AGN)] = \log[\nu L_\nu(6.0\ \mu m)] + 0.32 \pm 0.06$. We make a nominal modification to this by transforming $\nu L_\nu(5.5\ \mu m)$ to $\nu L_\nu(6.0\ \mu m)$ using Markarian 231 because of its similarity to the average spectrum of our absorbed sources in Figure 10. With this correction, we have $\log[L_{ir}(AGN)] = \log[\nu L_\nu(5.5\ \mu m)] + 0.33 \pm 0.06$. We adopt this relation as applying to a "pure" AGN, with no contribution to infrared luminosity from any source other than the torus heated by the AGN.

These two relations for deriving L_{ir}(SB) and L_{ir}(AGN) are used to determine the starburst and AGN luminosities for the FSC sources. Results are in Table 3 and Figure 10. We find that sources divide equally between those dominated by AGN luminosity and those by starburst luminosity. It is notable in Figure 10 that the median luminosity in the sample attributed to AGN, log L_{ir}(AGN) ~ 45.2, is the same as that attributed to starbursts, log L_{ir}(SB), although AGN sources reach to higher luminosities.

3.5. Radio Characteristics

Because this FSC sample was selected with the requirement of a FIRST radio detection (White et al. 1997), all sources have 1.4 GHz detections. We list in Table 2 the values of the parameter q, defined as q = $\log[f_\nu(25\ \mu\mathrm{m})/f_\nu(1.4\ \mathrm{GHz})]$ in the observed frame. For determining q, sources are assumed to be unresolved so the peak $f_\nu(1.4\ \mathrm{GHz})$ is used. For the FSC sources, the peak flux typically differs by $\sim 10\%$ from integrated fluxes. As discussed in section 3.1, the much higher S/N and higher spatial resolution of the *Spitzer* detections gives more accurate photometry at 25 μm than the IRAS FSC fluxes so the IRS $f_\nu(25\ \mu\mathrm{m})$ are used to determine q.

The comparison of q and $\nu L_\nu(5.5\ \mu\mathrm{m})$ is shown in Figure 11. Larger values of q correspond to relatively weaker radio sources. The median value of q for the FSC sample is 1.25. This is larger than the median of q = 0.8 for faint *Spitzer* First Look Survey sources detected at both 24 μm and 1.4 GHz (Appleton et al. 2004), which is the q value expected from previously known radio-infrared correlations for starbursts (Condon et al. 1982). The median q is even less, q = 0.4, for faint sources in the *Spitzer* First Look Survey which have IRS spectra and z > 1 in Weedman et al. (2006c). Some of these differences may be redshift effects. For example, Markarian 231 (shown in Figure 9) has q = 1.6 but, if at z = 2, would have q = 0.6.

The results in Fig. 11 do not indicate that the value of q can be used as a discriminant between starburst and AGN sources. A median q of ~ 1.3 is found both for the starburst sources that have PAH features and for the remaining sources dominated by AGN. Also, the range of q is similar for both categories of sources. All of the values of q for the FSC sources are much larger than in radio-loud AGN or quasars, for which q < -1 at any redshift (Higdon et al. 2005). The radio data, therefore, do not indicate any evidence of radio-loud AGN among the FSC sources.

4. Summary

The IRAS Faint Source Catalog (FSC) was used to select the 31 optically faintest FSC sources which are also identified in the FIRST radio survey, representing the optically faintest 1% of IRAS extragalactic sources. 28 of these sources have been observed with the Infrared Spectrograph on *Spitzer*. *Spitzer* fluxes indicate that about half of the sources have f_ν(25 μm) which are below the IRAS FSC flux limit. This indicates that about half of the optically faint sources taken from the FSC are actually spurious FSC detections. These sources are nevertheless detected by *Spitzer* because the presence of a FIRST radio source also provides an infrared source of sufficient brightness for a *Spitzer* detection.

This FSC sample reaches to higher redshifts and higher luminosities than the IRAS-discovered ULIRG samples observed spectroscopically with *Spitzer*, and overlaps the luminosity range of *Spitzer*-discovered 24 μm sources at z $\sim$ 2. The FSC sources have 0.12 $<$ z $<$ 1.0 and luminosities 43.3 $< \log[\nu L_\nu(5.5~\mu m)] <$ 46.7. 15 of the sources have detectable PAH features, and 19 have measurable silicate absorption. Median properties of the sample having silicate absorption are very similar to the ULIRG Markarian 231 in silicate strength, continuum luminosity, ratio $f_\nu(25~\mu m)/f_\nu(J)$, and relative radio luminosity.

PAH luminosities are used to determine the starburst luminosity within each source, and predictions from dusty torus models are used to determine the AGN luminosity. Sources have similar bolometric luminosities arising from starbursts and from AGN and are equally divided between sources dominated by starbursts and sources dominated by AGN. The ratio of infrared to radio flux is not a measure of whether sources are dominated in the infrared by starburst or AGN luminosity.

We thank Don Barry for technical assistance. This work is based on observations made with the Spitzer Space Telescope, which is operated by the Jet Propulsion Laboratory, California Institute of Technology under NASA contract 1407. Support for this work by the IRS GTO team at Cornell University was provided by NASA through Contract Number 1257184 issued by JPL/Caltech. Support was also provided by the US Civilian Research and Development Foundation under grant ARP1-2849-YE-06. This research has made use of the NASA/IPAC Extragalactic Database (NED) which is operated by the Jet Propulsion Laboratory, California Institute of Technology, under contract with the National Aeronautics and Space Administration.

REFERENCES

Appleton, P.N., et al. 2004, ApJS, 154, 147

Armus, L. et al. 2007, ApJ, 656, 148

Becker R.H., Helfand D.J., and White, R.L. 1997, AJ, 475, 479

Brand, K. et al. 2007, ApJ, 663, 204

Brandl, B. et al. 2006, ApJ, 653, 1129

Cabanela, J. E., Humphreys, R. M., Aldering, G., Larsen, J. A., Odewahn, S. C., Thurmes, P. M., and Cornuelle, C. S. 2003, PASP, 115, 837

Condon, J.J., Condon M.A., Gisler, G., and Puschell, J. 1982, ApJ, 252, 102

Desai, V. et al. 2007, ApJ, in press, (astro-ph 07074190)

Farrah, D., Afonso, J., Efstathiou, A., Rowan-Robinson, M., Fox, M., and Clements, D. 2003, MNRAS, 343, 585

Farrah, D. et al. 2007, ApJ, 667, 149

Farrah, D. et al, 2008, ApJ, in press

Fiore, F. et al. 2007, ApJ, in press, (astro-ph 07052864)

Genzel, R. et al. 1998, ApJ, 498, 579

Hao, L.,Weedman, D.W., Spoon, H.W.W., Marshall, J. A., Levenson, N. A., Elitzur, M., and Houck, J. R. 2007, ApJ, 655, L77

Higdon, S.J.U., et al. 2004, PASP, 116, 975

Higdon, J.L., et al. 2005, ApJ, 626, 58

Hönig, S. F., Beckert, T., Ohnaka, K., and Weigelt, G. 2006, A&A, 452, 459

Houck, J. R., et al. 2004, ApJS, 154, 18

Houck, J.R. et al. 2005, ApJ, 622, 105

Houck, J.R., Weedman, D.W., Le Floc'h, E., and Hao, L. 2007, ApJ, 671, 323

Humphreys, R.H., Landau, R., Ghigo, F.D., Zumach, W., and Labonte, A.E. 1991, AJ, 102, 395

Imanishi, M., Dudley, C. C., Maiolino, R., Maloney, P. R., Nakagawa, T., and Risaliti, G. 2007, ApJ, in press, (astro-ph/0702136)

Kim, D.-C., Veilleux, S., and Sanders, D. B. 1998, ApJ, 508, 627

Laurent, O., Mirabel, I. F., Charmandaris, V., Gallais, P., Madden, S. C., Sauvage, M., and Vigroux, L. 2000, A&A, 359, 887

Levenson, N. A., Sirocky, M. M., Hao, L., Spoon, H. W. W., Marshall, J. A., Elitzur, M., and Houck, J. R. 2007, ApJ, 654, L45

Marshall, J.A., Herter, T.L., Armus, L., Charmandaris, V., Spoon, H.W.W., Bernard-Salas, J., and Houck, J.R. 2007, ApJ, in press (astro-ph 07072962)

Moshir, M. et al. 1990, IRAS Faint Source Survey Catalog, National Space Science Data Center

Perry, J.J, Burbidge, E.M, and Burbidge, G.R. 1978, PASP, 90, 337

Polletta, M., Weedman, D., Hönig, S., Lonsdale, C. J., Smith, H. E., and Houck, J. 2007, ApJ, in press, (astro-ph 07094458)

Pope, A. et al. 2008, ApJ, in press (astro-ph 07111553)

Rieke, G.H. et al., 2004, ApJS, 154, 25

Sajina, A., Yan, L., Armus, L., Choi, P., Fadda, D., Helou, G., and Spoon, H. 2007, ApJ, 664, 713

Skrutskie, M.F. et al. 2006, AJ, 131, 1163

Spoon, H.W.W. et al 2007, ApJ, 654, L49

Urrutia, T., Lacy, M., Gregg, M.D., and Becker, R.H. 2005, ApJ, 627, 75

White, R. L., Becker, R. H., Helfand, D. J., and Gregg, M. D. 1997, ApJ, 475, 479

Weedman, D. W. et al. 2005, ApJ, 633, 706

Weedman, D. et al. 2006a, ApJ, 656, 101

Weedman, D.W. et al. 2006b,ApJ, 651, 101

Weedman, D. W.; Le Floc'h, E.; Higdon, S. J. U.; Higdon, J. L.; Houck, J. R. 2006c, ApJ, 638, 613

Yan, L. et al. 2007, ApJ, 658, 778

This preprint was prepared with the AAS LATEX macros v5.2.

Table 1. IRS Observations of Sources

Number	Source Name[a]	coordinates[b] FIRST J2000	AOR	program	time[c] s	date[d] mo/day/yr
1	FSC 07247+6124	072912.10+611853.5	17540096	30121	120,60	11/16/06
2	FSC 09105+4108	091345.28+405632.6	7771392	1018	120,180	11/29/03
3	FSC 09121+2430	091501.71+241812.2	17540352	30121	84,60	05/01/07
4	FSC 09235+5425	092703.07+541206.6	17540608	30121	120,60	11/17/06
5	FSC 09284+0413	093101.27+035955.2	17540864	30121	84,60	06/09/07
6	FSC 09425+1751	094521.36+173753.4	17541120	30121	84,60	06/08/07
7	FSC 10219+2657	102447.39+264209.0	17541888	30121	84,60	12/25/06
8	FSC 11257+5113	112832.73+505721.1	17542400	30121	120,60	05/02/07
9	FSC 13080+3237	131028.64+322049.2	17542912	30121	120,60	06/27/06
10	FSC 13297+4907	133150.54+485150.6	17543168	30121	120,60	06/27/06
11	FSC 14448-0141	144727.54-015330.3	17543424	30121	120,60	07/25/06
12	FSC 14475+1418	144954.86+140610.5	17543680	30121	120,60	07/29/06
13	FSC 14481+4454	144953.70+444150.3	17543936	30121	120,60	07/04/06
14	FSC 14503+6006	145135.04+595437.6	17544192	30121	120,60	07/04/06
15	FSC 14516+3851	145335.96+383913.1	17544448	30121	120,60	06/24/06
16	FSC 14589+2329	150113.19+232908.2	4169216	49	56,120	02/07/04
17	FSC 15065+3852	150825.42+384122.1	17544704	30121	120,60	07/01/06
18	FSC 15307+3252	153244.05+324246.7	4983552	105	360,480	03/04/04
19	FSC 15385+4320	154014.02+431042.4	17544960	30121	120,60	06/25/06
20	FSC 15458+0041	154823.38+003212.8	17545216	30121	120,60	03/20/07
21	FSC 15492+3454	155108.86+344533.6	17545472	30121	120,60	06/25/06
22	FSC 15496+0331	155206.16+032244.0	17545728	30121	120,60	03/16/07
23	FSC 15585+4518	160003.29+451046.2	17545984	30121	120,60	07/24/06
24	FSC 16001+1652	160222.38+164354.3	17546240	30121	120,60	03/10/07
25	FSC 16073+0209	160949.75+020130.8	17546496	30121	120,60	03/18/07
26	FSC 16156+0146	161809.36+013922.1	17546752	30121	120,60	09/17/06
27	FSC 16242+2218	162626.00+221145.9	17547008	30121	120,60	09/17/06
28	FSC 17233+3712	172507.40+370932.1	4986880	105	360,480	06/07/04

[a]Source name from the IRAS Faint Source Catalog.

[b]Coordinates for the FIRST source which is closest to the FSC source.

[c]Total integration time for IRS short low modules (first number) and long low modules (second number).

[d]Date of IRS observation

Table 2. Observed Properties of Sources

No.	Source	z	f_ν(25 μm) IRAS mJy	f_ν(25 μm) IRS mJy	E[a] mag	J[b] mag	f_ν(1.4 GHz) mJy	q[c]	f_ν(5.5 μm) mJy	f_ν(15 μm) mJy	EW(6.2μm) μm	f(6.2μm)[d]	f(11.3μm)[d]	τ_{si}[e]
1	07247	0.137	175	119	18.0	16.08	3.13	1.57	4.1	47.2	0.08±0.01	2.94±0.42	2.48±0.46	-0.31
2	09105	0.446	333	333	18.1	16.83	5.79	1.76	54	297	< 0.002	< 1.3	< 0.2	-0.34
3	09121	0.84[f]	179	100	20.0	16.56	9.80	1.01	42.5	119	< 0.01	< 1.8	< 0.4	0.0
4	09235	0.123	136	97	18.3	16.75	3.31	1.47	2.0	42.8	0.19±0.02	4.62±0.47	2.67±0.16	0.0
5	09284	0.146	147	25	18.2	16.11	1.05	1.38	1.5	6.9	0.56±0.03	12.14±0.73	10.0±0.2	0.0
6	09425	0.130	436	322	18.6	15.72	38.7	0.92	17.8	162	< 0.1	< 0.3	< 3.91	-0.78
7	10219	0.225	151	28	18.8	16.77	1.68	1.22	1.3	11.8	0.29±0.04	4.53±0.7	3.92±0.5	0.0
8	11257	0.197	123	75	18.4	16.55	1.77	1.63	3.0	35.8	0.07±0.01	3.12±0.6	1.91±0.4	-0.51
9	13080	0.997[f]	271	9.0	19.2	16.34	···	···	3.5	10.3	···	···	···	0.0
10	13297	0.128	139	102	18.5	16.68	1.17	1.94	3.6	53.1	< 0.05	< 1.8	< 1.5	-0.69
11	14448	0.210	176	38	18.9	> 17.7	1.78	1.33	3.8	23.4	< 0.02	<0.9	2.01±0.65	-0.62
12	14475	0.251	143	114	18.5	16.68	12.8	0.95	11.6	91	0.03±0.005	3.4±0.52	< 3.2	-0.89
13	14481	0.670	85	64	21.0	> 17.7	10.7	0.78	19.2	67.6	< 0.006	< 1.1	< 0.5	0.0
14	14503	0.577	79	58	21.0	> 17.7	16.3	0.55	8.4	60	< 0.02	< 1.9	< 1.0	-1.01
15	14516	0.153	85	24	19.3	16.77	2.07	1.06	0.75	9.4	0.20±0.03	2.24±0.38	2.49±0.14	-0.87
16	14589	0.261	84	53	17.8	15.98	4.49	1.07	11.7	37.8	< 0.017	< 1.73	< 3.4	-0.24
17	15065	0.355	82	45	20.2	> 17.7	2.43	1.27	4.9	32.9	< 0.013	< 0.84	4.41±0.27	-0.59
18	15307	0.927	71	46	19.0	> 17.7	5.7	0.91	9.4	70.0	< 0.006	< 0.5	< 2.4	-0.32
19	15385	0.380	92	76	18.5	> 17.7	1.10	1.84	6.0	54.6	0.02±0.005	1.22±0.34	< 1.1	0.0
20	15458	0.254	126	40	18.7	16.70	2.53	1.20	4.3	25.2	< 0.01	< 0.59	< 0.26	0.0
21	15492	0.311	80	40	19.6	> 17.7	1.08	1.57	6.0	29.7	< 0.02	< 0.9	1.56±0.42	-1.46
22	15496	0.193	144	122	18.5	16.20	28.5	0.63	13.7	86.7	< 0.01	< 1.8	2.39±0.47	-1.10
23	15585	0.486	64	11.0	20.0	> 17.7	1.58	0.87	3.1	11.9	0.10±0.04	2.0±0.82	3.25±0.51	-2.2
24	16001	0.672	144	104	18.1	16.62	1.90	1.74	22.9	109	< 0.01	< 0.25	< 1.29	0.0
25	16073	0.223	153	123	19.2	17.46	5.41	1.36	9.6	96	0.06±0.002	7.5±0.3	< 4.1	-1.5
26	16156	0.133	279	261	18.3	16.57	7.9	1.52	27	154	< 0.01	< 2.8	< 0.8	-2.6
27	16242	0.157	71	31	19.5	> 17.7	1.39	1.35	1.3	15.1	< 0.01	< 0.25	1.07±0.12	-2.7
28	17233	0.702	50	29	21.0	> 17.7	3.16	0.96	1.7	34.3	< 0.04	< 0.78	< 1.2	-0.51

[a]Photographic E magnitude from APS.

[b]J magnitude from 2MASS (Skrutskie et al. 2006).

[c]q = log[f_ν(25 μm)/f_ν(1.4 GHz)] in observed frame, using f_ν(1.4 GHz) of "peak flux" from FIRST, corresponding to an unresolved source.

[d]Total flux of feature in units of 10^{-21} W cm^{-2}, fit with single Gaussian. Uncertainties in fluxes and equivalent widths are statistical uncertainties from fitting of feature and do not include systematic uncertainties of $\lesssim$ 10% which may arise from fitting procedure chosen, as discussed in text.

[e]τ_{si} is measure of depth of 9.7 μm absorption feature, defined as $\tau_{si} = \ln[f_\nu(\mathrm{abs})/f_\nu(\mathrm{cont})]$, for f_ν(abs) measured at the maximum depth of absorption and f_ν(cont) the unabsorbed continuum as extrapolated in Spoon et al. (2007).

[f]Redshift for no. 3, a red quasar, is optical redshift from Urrutia et al. (2005), and for number 9, a blazar, is from Perry et al. (1978); other redshifts are determined from the IRS spectra.

Table 3. Luminosities of Sources

Number	Source	D_L[a] Mpc	$\log[\nu L_\nu(5.5\ \mu m)]$ ergs s^{-1}	$\log[\nu L_\nu(15\ \mu m)]$ ergs s^{-1}	log[L(6.2)] ergs s^{-1}	log[L(6.2+11.3)] ergs s^{-1}	log[L(SB)][b] ergs s^{-1}	log[L(AGN)][c] ergs s^{-1}	L(SB)/[L(SB)+L(AGN)][d]
1	07247	637	43.98	44.60	42.15	42.42	44.85	44.31	> 0.78
2	09105	2460	46.17	46.47	<42.96	<43.03	<45.66	46.50	< 0.13
3	09121	5340	46.63	46.64	<43.79	<43.88	<46.49	46.96	< 0.25
4	09235	565	43.58	44.46	42.25	42.44	44.95	43.91	> 0.92
5	09284	683	43.60	43.83	42.83	43.09	45.53	43.93	> 0.98
6	09425	602	44.57	45.09	<41.10	<42.26	<43.80	44.90	< 0.07
7	10219	1108	43.93	44.45	42.82	43.09	45.52	44.26	> 0.95
8	11257	952	44.17	44.81	42.53	42.73	45.23	44.50	> 0.84
9	13080	6610	45.70	45.73	...	...	...	...	...
10	13297	594	43.87	44.60	<41.87	<42.14	<44.57	44.20	< 0.70
11	14448	1025	44.34	44.68	<42.05	<42.56	<44.75	44.67	< 0.55
12	14475	1254	44.98	45.43	42.80	<43.09	45.50	45.31	> 0.61
13	14481	4036	46.08	46.20	<43.33	<43.50	<46.03	46.41	< 0.29
14	14503	3360	45.59	46.01	<43.41	<43.59	<46.11	45.92	< 0.60
15	14516	719	43.34	44.00	42.14	42.46	44.84	43.67	> 0.94
16	14589	1310	45.01	45.09	<42.55	<43.02	<45.25	45.34	< 0.44
17	15065	1870	44.92	45.31	<42.54	43.34	45.24	<45.25	< 0.50
18	15307	6030	46.06	46.50	<43.32	<44.09	<46.02	46.39	< 0.30
19	15385	2030	45.07	45.59	42.78	<43.06	45.48	45.40	> 0.55
20	15458	1270	44.55	44.89	<42.05	<42.21	<44.75	44.88	< 0.43
21	15492	1606	44.89	45.14	<42.43	<42.87	<45.13	45.22	< 0.45
22	15496	930	44.81	45.18	<42.26	<42.63	<44.96	45.14	< 0.40
23	15585	2730	45.01	45.15	43.25	43.67	45.95	45.34	> 0.80
24	16001	4050	46.17	46.41	<42.69	<43.48	<45.39	46.50	< 0.07
25	16073	1090	44.78	45.35	43.03	<43.22	45.73	45.11	> 0.80
26	16156	620	44.78	45.09	<42.11	<42.22	<44.81	45.11	< 0.34
27	16242	740	43.59	44.24	<41.22	<41.94	<43.92	43.92	< 0.50
28	17233	4270	45.07	45.94	<43.23	<43.64	<45.93	45.40	< 0.77

[a]uminosity distance determined by E.L. Wright, http://www.astro.ucla.edu~wright/CosmoCalc.html, for $H_0 = 71\ \mathrm{km\,s^{-1}\,Mpc^{-1}}$, Ω_M=0.27 and Ω_Λ=0.73.

[b]Total luminosity of starburst, assuming that $\log[L_{ir}(SB)] = \log[L(6.2)] + 2.7\pm0.1$, from Brandl et al.(2006) and Pope et al.(2007).

[c]Total luminosity from dusty torus of AGN, assuming $\log[L_{ir}(AGN)] = \log[\nu L_\nu(5.5\ \mu m)] + 0.33\pm0.06$, from Polletta et al.(2007) and assuming that all continuum luminosity $\nu L_\nu(5.5\ \mu m)$ arises from an AGN.

[d]Fraction of total luminosity which arises from a starburst. If a PAH feature is detected, this fraction is shown as a lower limit because some of the continuum at 5.5 μm which is attributed to an AGN actually arises from the starburst. If no PAH feature is detected, this fraction is shown as an upper limit because there is no direct evidence that a starburst is present. Source 9 is a blazar so the parameters for determining L_{ir}(AGN) and L_{ir}(SB) are not applicable.

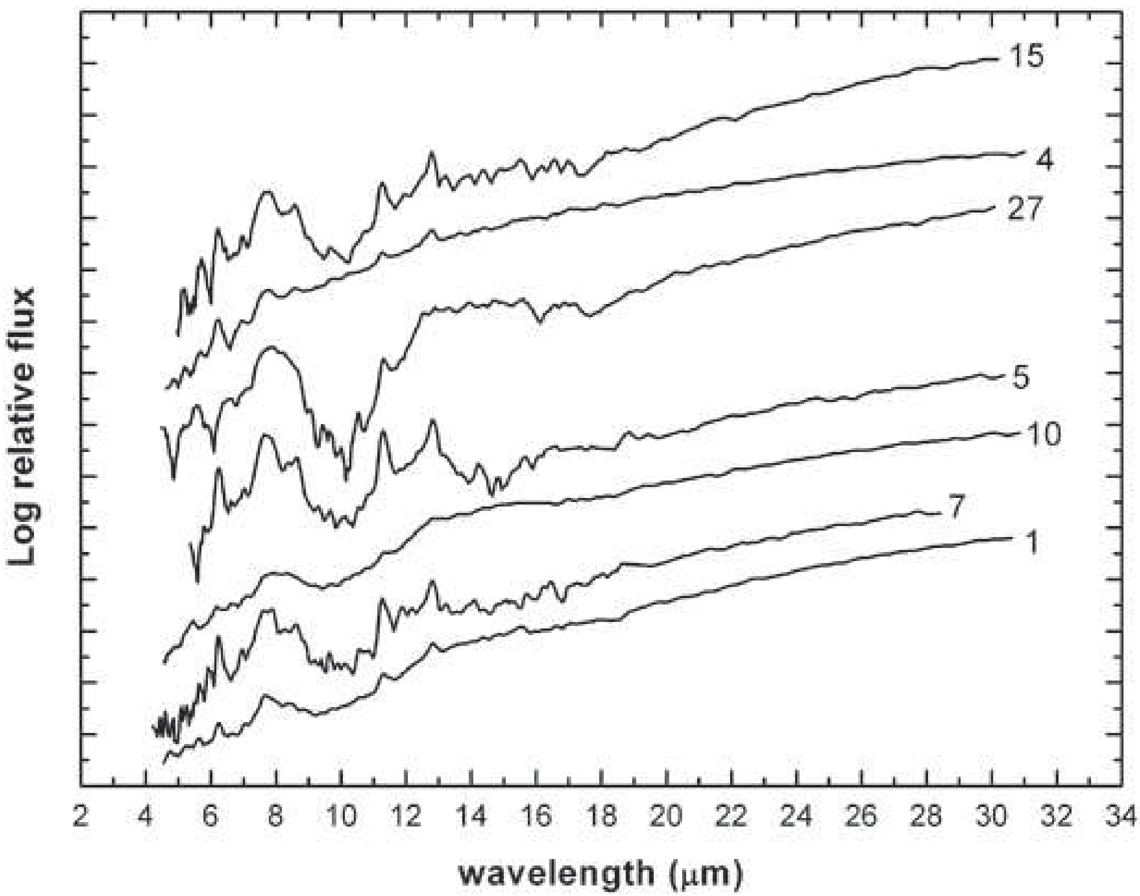

Fig. 1.— IRS spectra of FSC sources in rest frame, ordered by $\nu L_\nu(5.5\ \mu m)$ in Table 3, lowest luminosity at the top. Sources of higher luminosity continue in Figure 2.

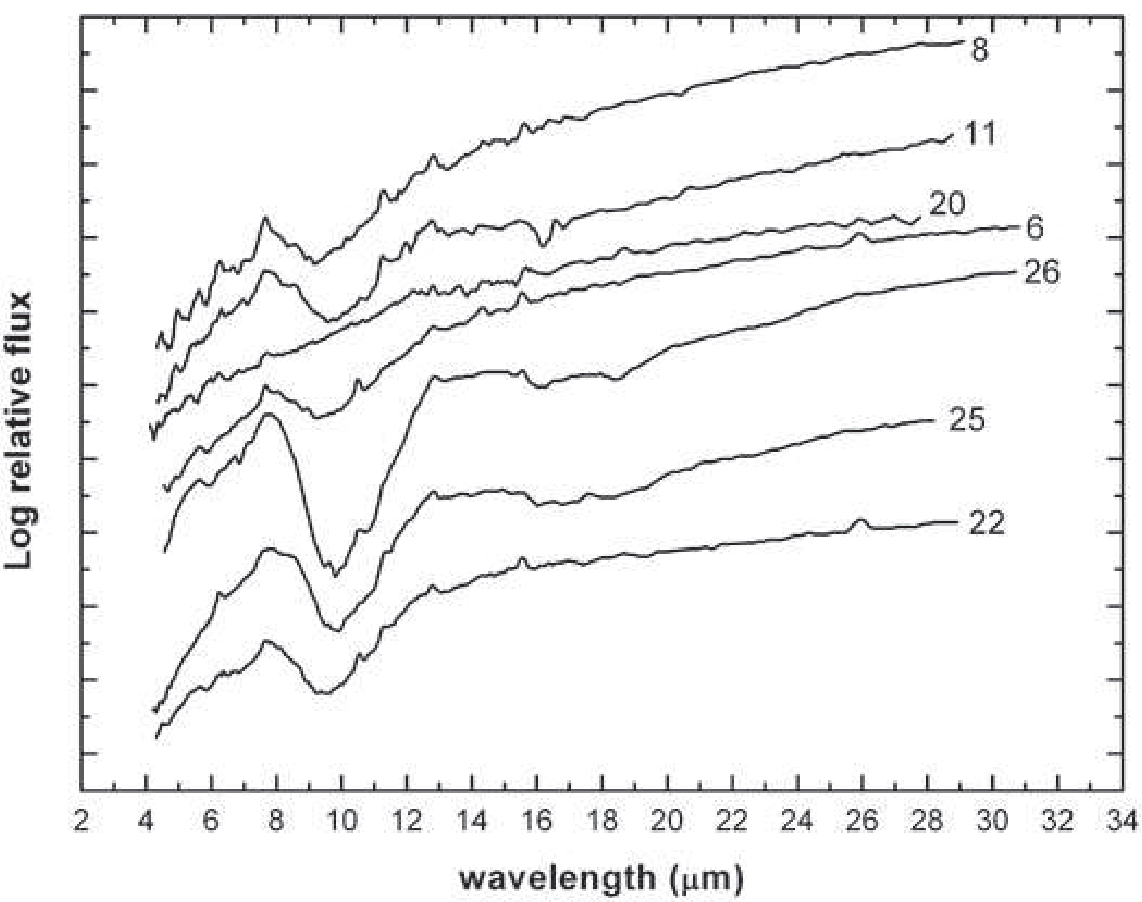

Fig. 2.— IRS spectra of FSC sources in rest frame, ordered by $\nu L_\nu(5.5\ \mu m)$ in Table 3, lowest luminosity at the top, continued from Figure 1. Sources of higher luminosity continue in Figure 3.

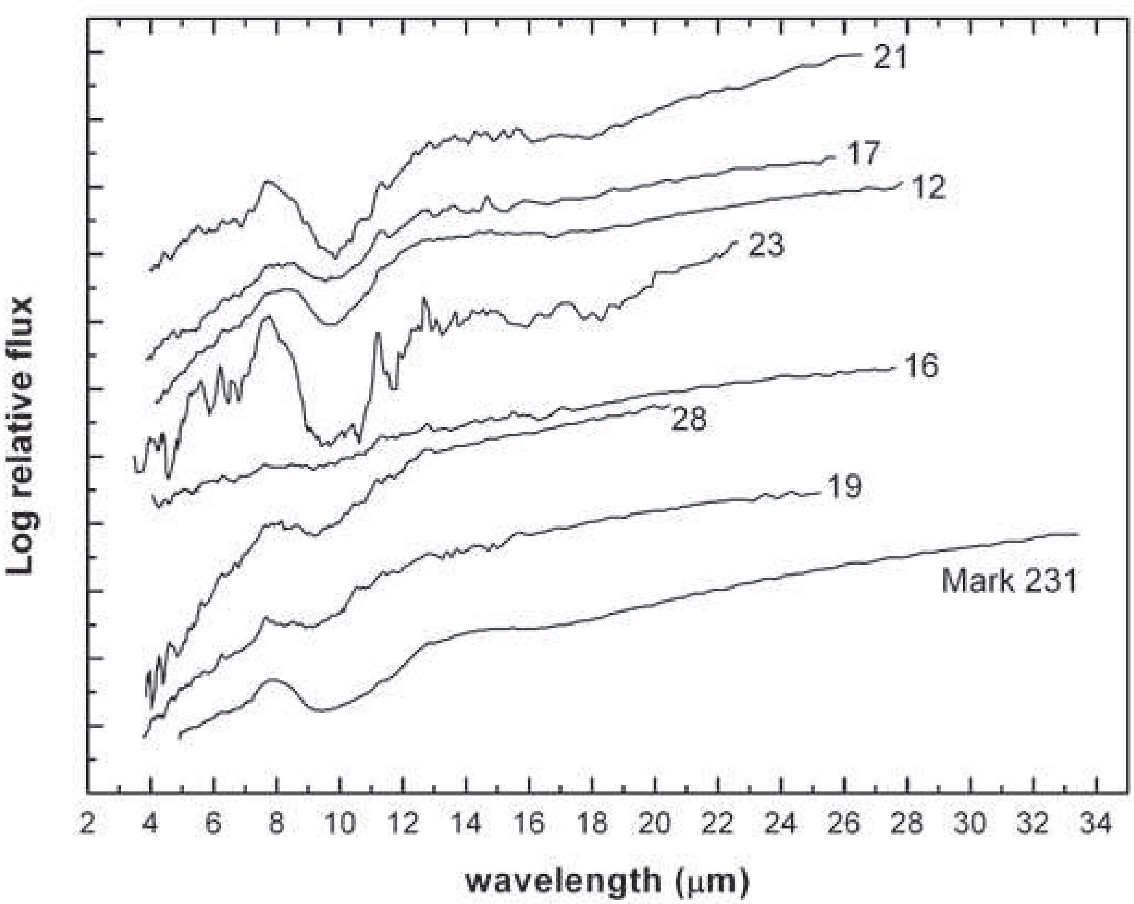

Fig. 3.— IRS spectra of FSC sources in rest frame, ordered by $\nu L_\nu(5.5\ \mu m)$ in Table 3, lowest luminosity at the top, continued from Figure 2. Sources of higher luminosity continue in Figure 4.

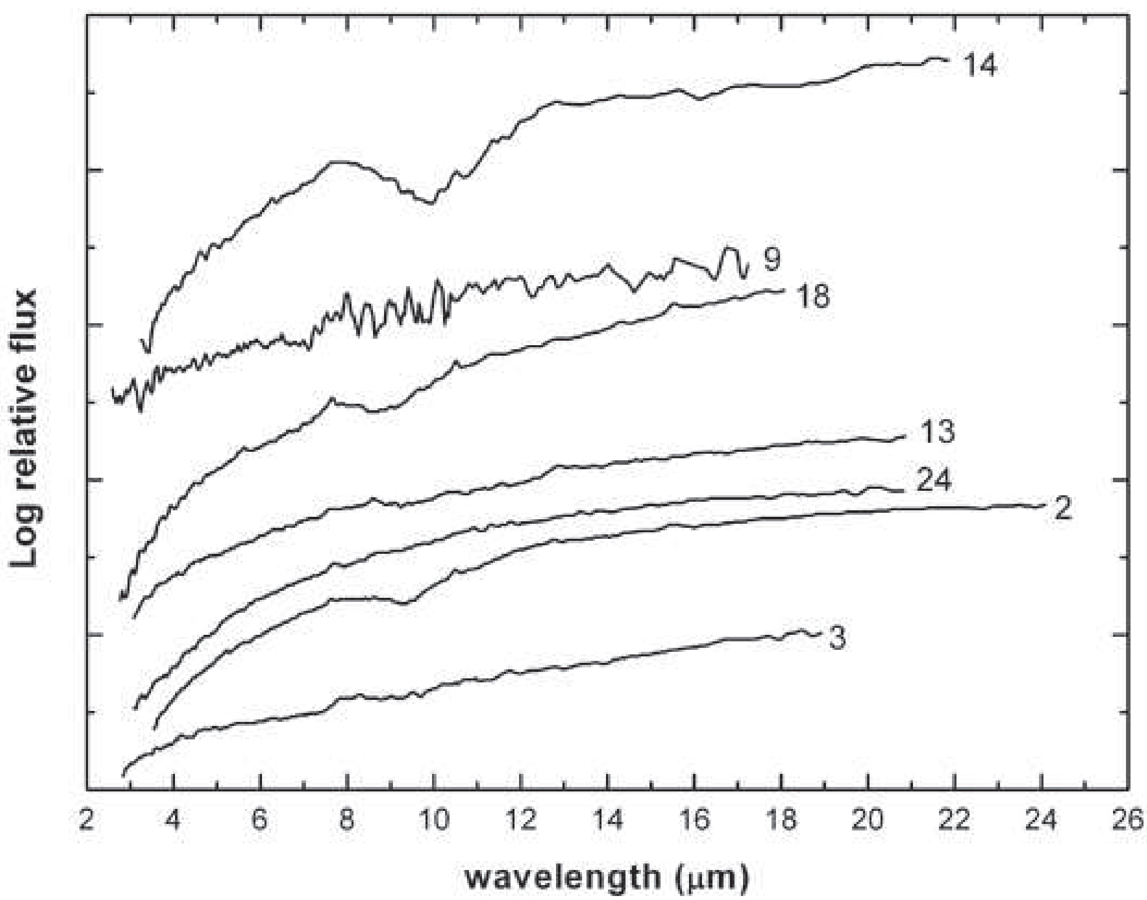

Fig. 4.— IRS spectra of FSC sources in rest frame, ordered by $\nu L_\nu(5.5\ \mu m)$ in Table 3, lowest luminosity at the top, continued from Figure 3. Source having highest luminosity is number 3.

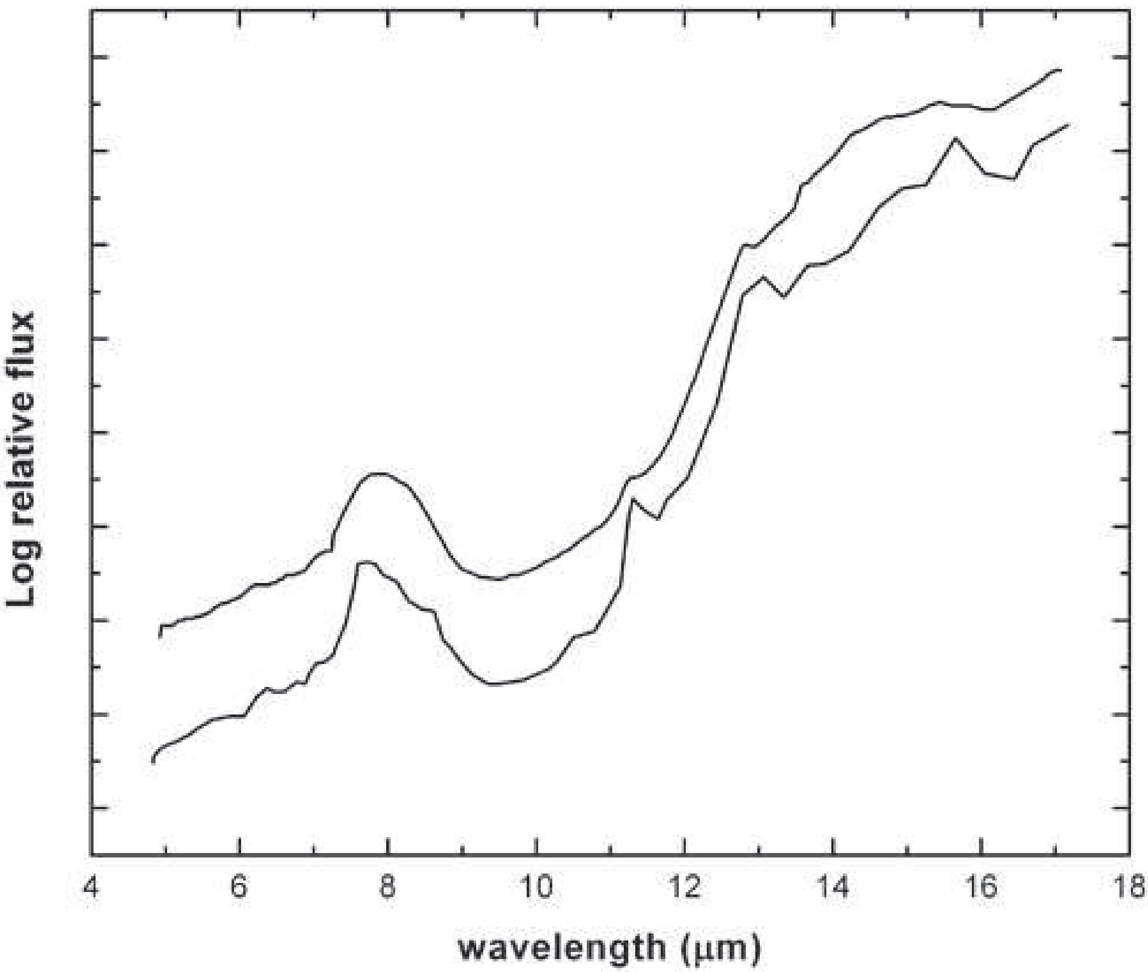

Fig. 5.— Comparison of Markarian 231 (top) with average of the 19 FSC galaxies in Table 1 with measured silicate absorption (bottom), arbitrarily normalized.

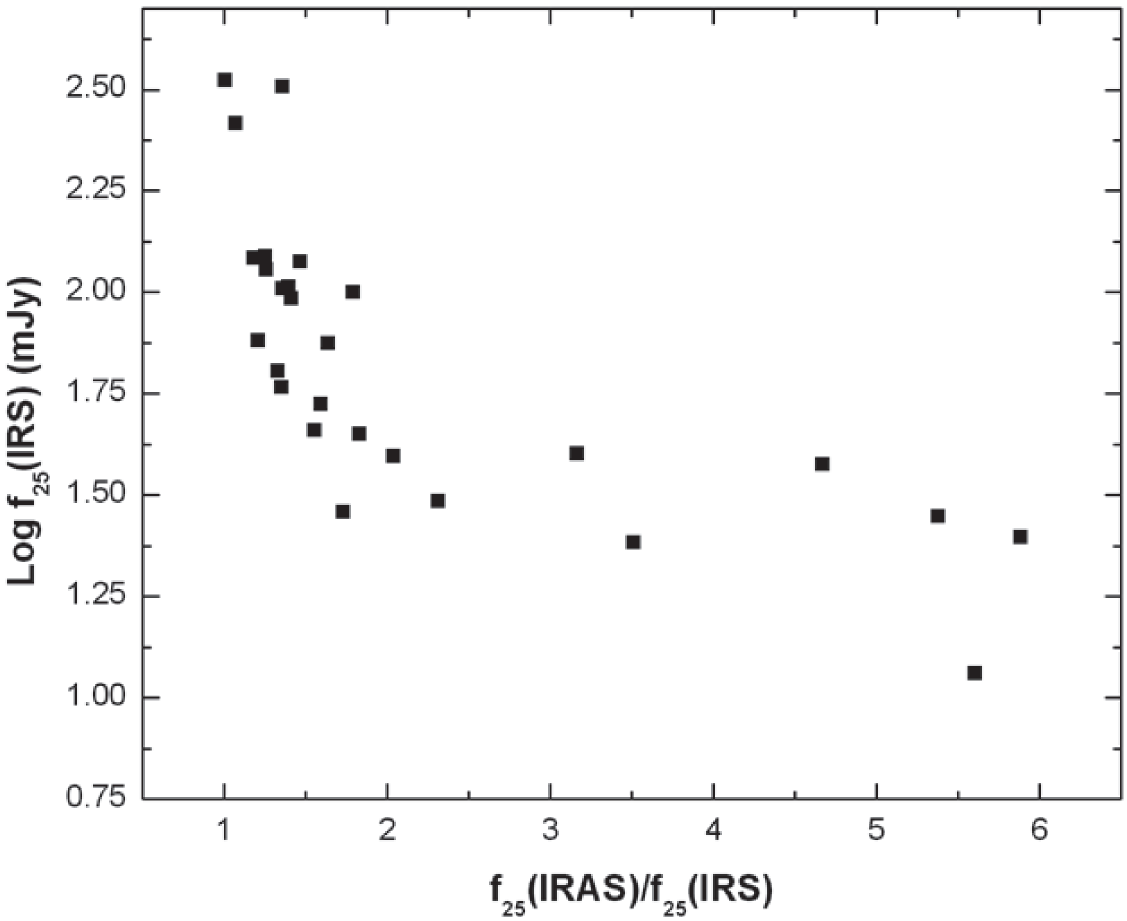

Fig. 6.— Comparison of $f_\nu(25\ \mu\text{m})$ measured with *Spitzer* IRS to $f_\nu(25\ \mu\text{m})$ listed in IRAS FSC for sources in Table 2. Uncertainties in IRS fluxes arise primarily from calibration uncertainties and are $\sim \pm\, 5\%$, comparable to the size of plotted symbols. Large discrepancies between IRS and IRAS fluxes for fainter sources are discussed in text as indication that many IRAS sources are spurious.

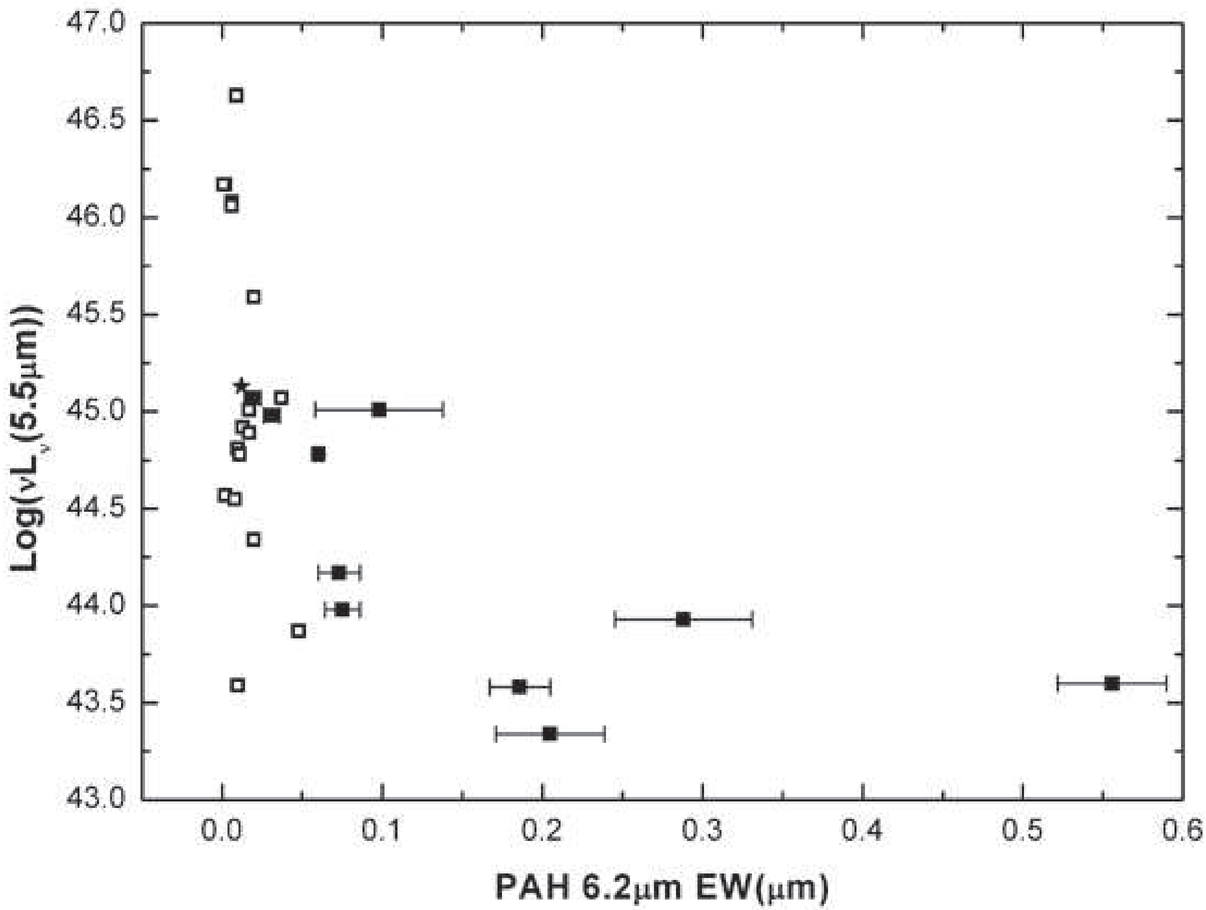

Fig. 7.— Comparison of luminosities and PAH strengths for FSC sources; filled squares are sources with PAH detections and open squares show PAH upper limits for sources without PAH detections. The star indicates Markarian 231. Error bars show uncertainties in PAH EWs from Table 2.

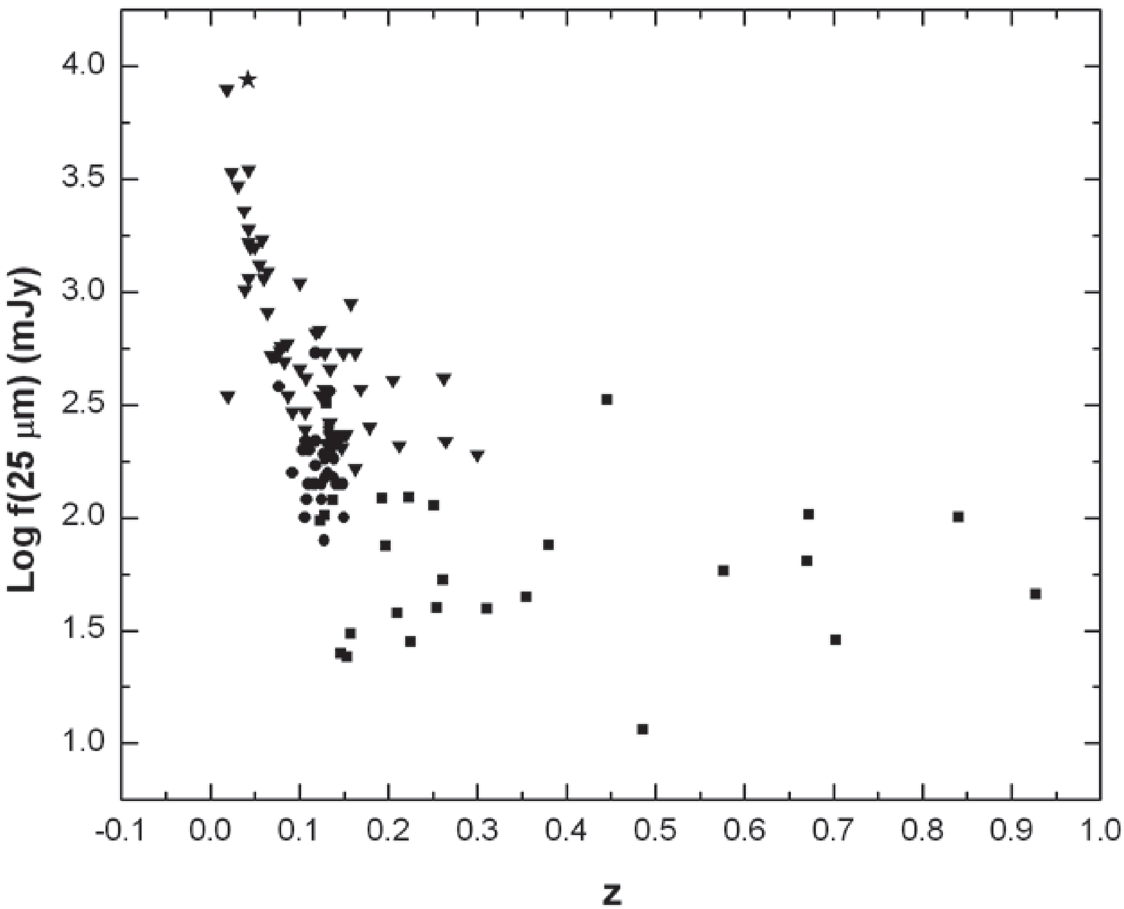

Fig. 8.— Distribution of redshift and $f_\nu(25\ \mu\mathrm{m})$ for ULIRG samples in Farrah et al. (2007)(filled triangles) and Imanishi et al. (2007) (filled circles) compared to FSC sample in present paper(filled squares). The star indicates Markarian 231. The $f_\nu(25\ \mu\mathrm{m})$ shown for ULIRGS are taken from IRAS fluxes; the $f_\nu(25\ \mu\mathrm{m})$ shown for FSC sources are synthetic $f_\nu(25\ \mu\mathrm{m})$ that should be observed by IRAS as determined from *Spitzer* IRS spectra. Uncertainties in IRS fluxes arise primarily from calibration uncertainties and are $\sim \pm 5\%$, comparable to the size of plotted symbols.

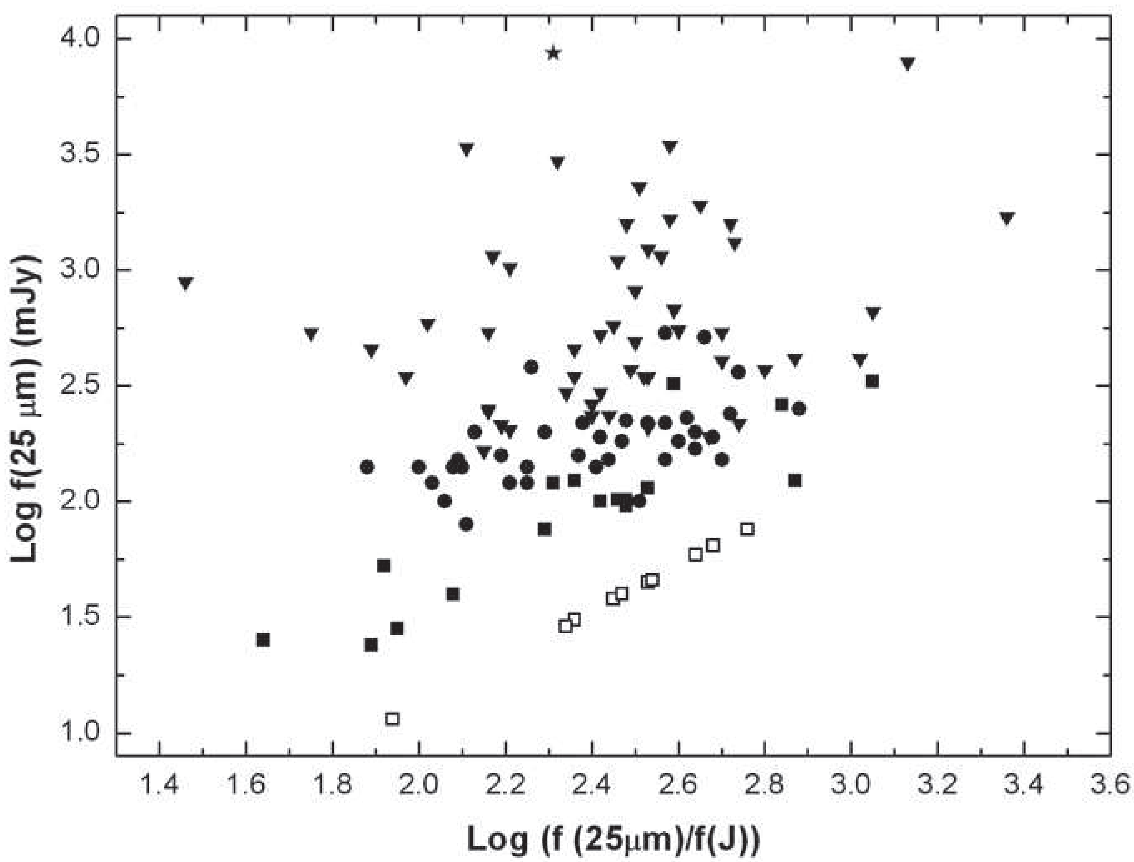

Fig. 9.— Comparison of mid-infrared and near-infrared (2MASS J) fluxes for ULIRG samples in Imanishi et al. (filled circles), Farrah et al.(filled triangles), and FSC sample in Table 2 (squares); open squares are limits for sources without J detections so the f(25 μm)/f(J) ratio is greater than shown. The star indicates Markarian 231. The f_ν(25 μm) shown for ULIRGS are taken from IRAS fluxes; the f_ν(25 μm) shown for FSC sources are synthetic f_ν(25 μm) that should be observed by IRAS as determined from *Spitzer* IRS spectra. Uncertainties in IRS fluxes arise primarily from calibration uncertainties and are $\sim \pm$ 5%, comparable to the size of plotted symbols.

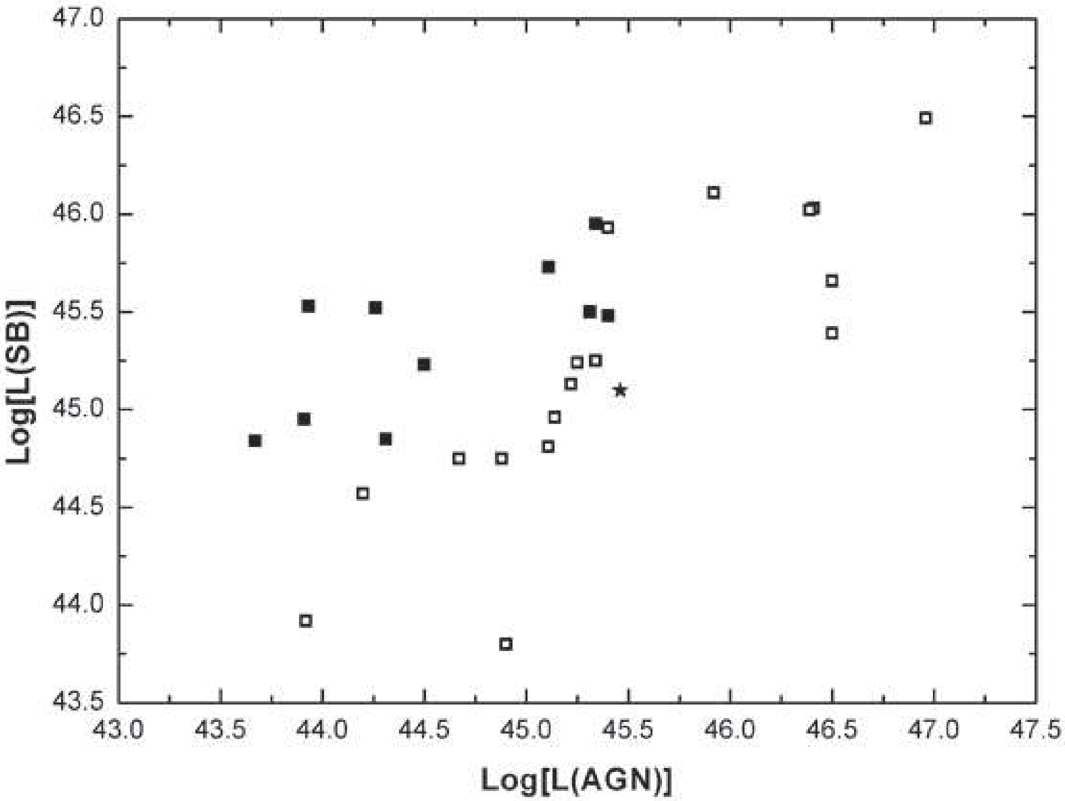

Fig. 10.— Comparison of bolometric luminosities from AGN with those from starbursts for FSC sample in Table 3, assuming that $\log[L_{ir}(SB)] = \log[L(6.2\ \mu m)] + 2.7$ for PAH luminosity L(6.2) and that $\log[L_{ir}(AGN)] = \log[\nu L_\nu(5.5\ \mu m)] + 0.33$ for continuum luminosity $\nu L_\nu(5.5\ \mu m)$. Filled squares are starbursts with PAH detections so the L(AGN) derived from continuum luminosities are upper limits for L(AGN) because some continuum may arise from the starburst; open squares are sources without PAH detections so the L(SB) derived from PAH luminosities are upper limits for L(SB) determined from upper limits on L(6.2). The star indicates Markarian 231.

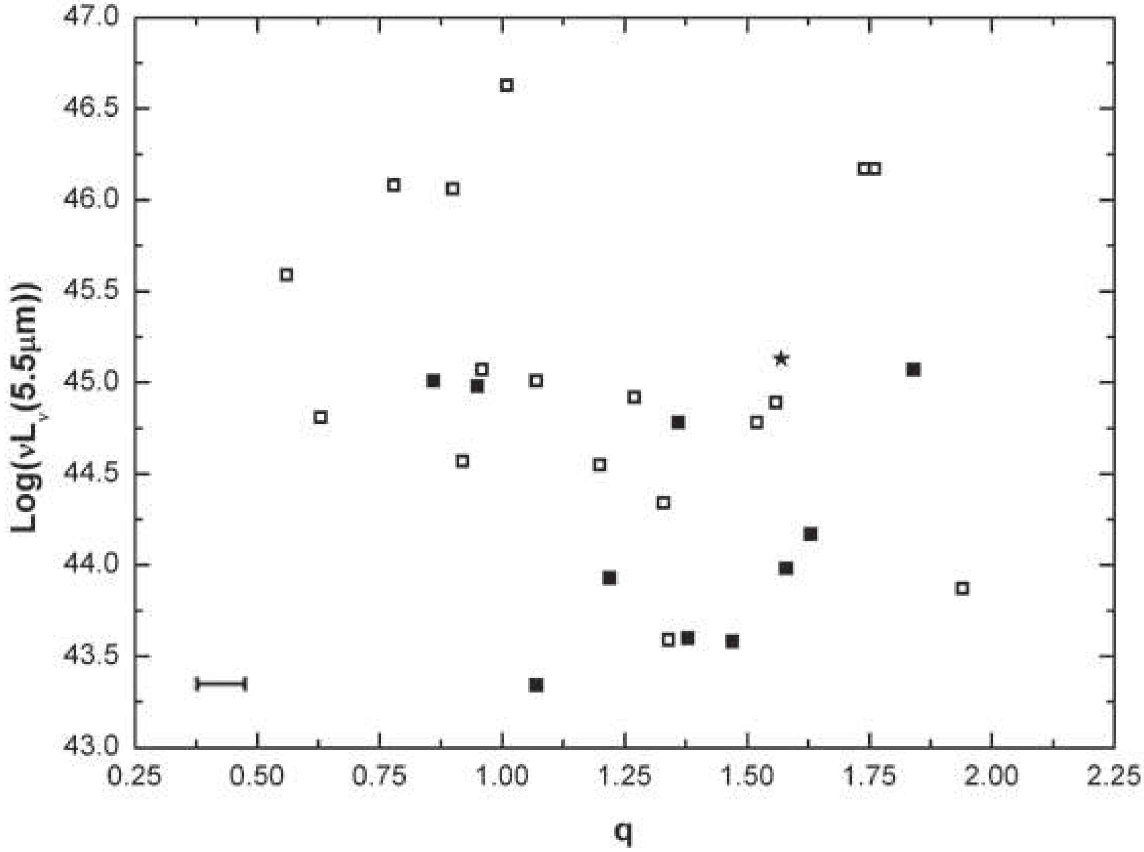

Fig. 11.— Comparison of luminosities and radio strength for FSC sources; q = log[f_ν(25 μm)/f_ν(1.4 GHz)] in observed frame. Filled squares are starburst sources (as defined by PAH detections), and open squares are AGN (no PAH detections). The star indicates Markarian 231. Uncertainties in q are typically ± 10%, shown by the representative error bar, arising primarily from uncertainty whether to adopt "peak" flux or "integrated" flux for the FIRST sources.